JCI The Journal of Clinical Investigation

Genetic reduction of eEF2 kinase alleviates pathophysiology in Alzheimer's disease model mice

Brenna C. Beckelman, … , Alexey G. Ryazanov, Tao Ma

J Clin Invest. 2019;129(2):820-833. https://doi.org/10.1172/JCI122954.

Research Article **Neuroscience**

Molecular signaling mechanisms underlying Alzheimer's disease (AD) remain unclear. Maintenance of memory and synaptic plasticity depend on de novo protein synthesis, dysregulation of which is implicated in AD. Recent studies showed AD-associated hyperphosphorylation of mRNA translation factor eukaryotic elongation factor 2 (eEF2), which results in inhibition of protein synthesis. We tested to determine whether suppression of eEF2 phosphorylation could improve protein synthesis capacity and AD-associated cognitive and synaptic impairments. Genetic reduction of the eEF2 kinase (eEF2K) in 2 AD mouse models suppressed AD-associated eEF2 hyperphosphorylation and improved memory deficits and hippocampal long-term potentiation (LTP) impairments without altering brain amyloid β (Aβ) pathology. Furthermore, eEF2K reduction alleviated AD-associated defects in dendritic spine morphology, postsynaptic density formation, de novo protein synthesis, and dendritic polyribosome assembly. Our results link eEF2K/eEF2 signaling dysregulation to AD pathophysiology and therefore offer a feasible therapeutic target.

Genetic reduction of eEF2 kinase alleviates pathophysiology in Alzheimer's disease model mice

Brenna C. Beckelman,[1] Wenzhong Yang,[1] Nicole P. Kasica,[1] Helena R. Zimmermann,[1] Xueyan Zhou,[1] C. Dirk Keene,[2] Alexey G. Ryazanov,[3] and Tao Ma[1,4,5]

[1]Department of Internal Medicine, Gerontology and Geriatric Medicine, Wake Forest School of Medicine, Winston-Salem, North Carolina, USA. [2]Department of Pathology, University of Washington School of Medicine, Seattle, Washington, USA. [3]Department of Pharmacology, Rutgers Robert Wood Johnson Medical School, Piscataway, New Jersey, USA. [4]Department of Physiology and Pharmacology, and [5]Department of Neurobiology and Anatomy, Wake Forest School of Medicine, Winston-Salem, North Carolina, USA.

Molecular signaling mechanisms underlying Alzheimer's disease (AD) remain unclear. Maintenance of memory and synaptic plasticity depend on de novo protein synthesis, dysregulation of which is implicated in AD. Recent studies showed AD-associated hyperphosphorylation of mRNA translation factor eukaryotic elongation factor 2 (eEF2), which results in inhibition of protein synthesis. We tested to determine whether suppression of eEF2 phosphorylation could improve protein synthesis capacity and AD-associated cognitive and synaptic impairments. Genetic reduction of the eEF2 kinase (eEF2K) in 2 AD mouse models suppressed AD-associated eEF2 hyperphosphorylation and improved memory deficits and hippocampal long-term potentiation (LTP) impairments without altering brain amyloid β (Aβ) pathology. Furthermore, eEF2K reduction alleviated AD-associated defects in dendritic spine morphology, postsynaptic density formation, de novo protein synthesis, and dendritic polyribosome assembly. Our results link eEF2K/eEF2 signaling dysregulation to AD pathophysiology and therefore offer a feasible therapeutic target.

Introduction

The molecular signaling mechanisms underlying Alzheimer's disease (AD) pathophysiology remain elusive, hindering the development of effective treatments. AD is characterized by profound memory loss and synaptic failure (1). A substantial body of evidence demonstrates that long-lasting forms of memory and synaptic plasticity require de novo protein synthesis, i.e., mRNA translation (2–6). Impaired translational capacity and ribosomal function have been observed in the brains of human AD patients, and recent studies indicate that protein synthesis impairments may contribute to cognitive defects in neurodegenerative diseases, such as AD, prion disease, and frontotemporal dementia (FTD) (7–11). Protein synthesis depends in part on eukaryotic elongation factor 2 (eEF2), which mediates the translocation step of elongation, catalyzing movement of tRNA from the ribosomal A-site to the P-site via GTP hydrolysis (12). Phosphorylation of eEF2 at Thr56 by its only known kinase, eEF2 kinase (eEF2K), disrupts peptide growth and represses general protein synthesis (12, 13). Abnormal hyperphosphorylation of eEF2 was observed in postmortem brain tissue from AD patients and in the brains of AD mouse models, but its link to AD-associated impairments of synaptic plasticity and memory is unknown (14, 15). Here, we aimed to determine whether genetic inhibition of eEF2K/eEF2 signaling could improve protein synthesis and alleviate pathophysiology in AD model mice.

Conflict of interest: The authors have declared that no conflict of interest exists.

Submitted: June 18, 2018; **Accepted:** November 27, 2018.
Reference information: *J Clin Invest*. 2019;129(2):820–833.
https://doi.org/10.1172/JCI122954.

Results

eEF2 hyperphosphorylation and de novo protein synthesis impairments in Tg19959 AD model mice are corrected by genetic reduction of eEF2K. By performing Western blot analysis on postmortem hippocampal tissue from human AD patients and age-matched controls, we found significantly increased levels of eEF2 phosphorylation at the Thr56 site (Figure 1A and Table 1). Moreover, we assayed postmortem human hippocampal tissues from patients with neuropathologically confirmed FTD and Lewy body dementia (LBD), 2 non-AD dementia syndromes (Tables 2 and 3). Notably, eEF2 was not hyperphosphorylated in either FTD or LBD tissues compared with their respective age-matched controls (Figure 1, B–C). Furthermore, immunohistochemical analysis of fixed postmortem brain sections from AD patients revealed increased levels of cytoplasmic phosphorylated eEFT (phospho-eEF2) throughout the AD hippocampus, including both neuronal soma and processes (Figure 1D). Next, we crossed Tg19959 AD model mice with a line of mice lacking eEF2K (*Eef2k*$^{+/-}$) to generate 4 genotypes: WT, Tg19959, heterozygous eEF2K$^{+/-}$ knockdown (eEF2K$^{+/-}$), and Tg19959/eEF2K$^{+/-}$ double-mutant (Tg/eEF2K$^{+/-}$) mice (Figure 1E). Both male and female mice aged 6 to 9 months were used for experimentation. As expected, Tg19959 mice showed significantly more eEF2 phosphorylation in hippocampal lysates than WT littermates (Figure 1E). Compared with that of Tg19959 mice, eEF2 phosphorylation in hippocampal lysates of Tg19959/eEF2K$^{+/-}$ mice was restored to WT levels (Figure 1E). The eEF2K reduction did not affect gross morphology of the hippocampus, nor did it impact total levels of eEF2 (Supplemental Figure 1, A–C; supplemental material available online with this article; https://doi.org/10.1172/JCI122954DS1). In addition, expression of the structural components of protein

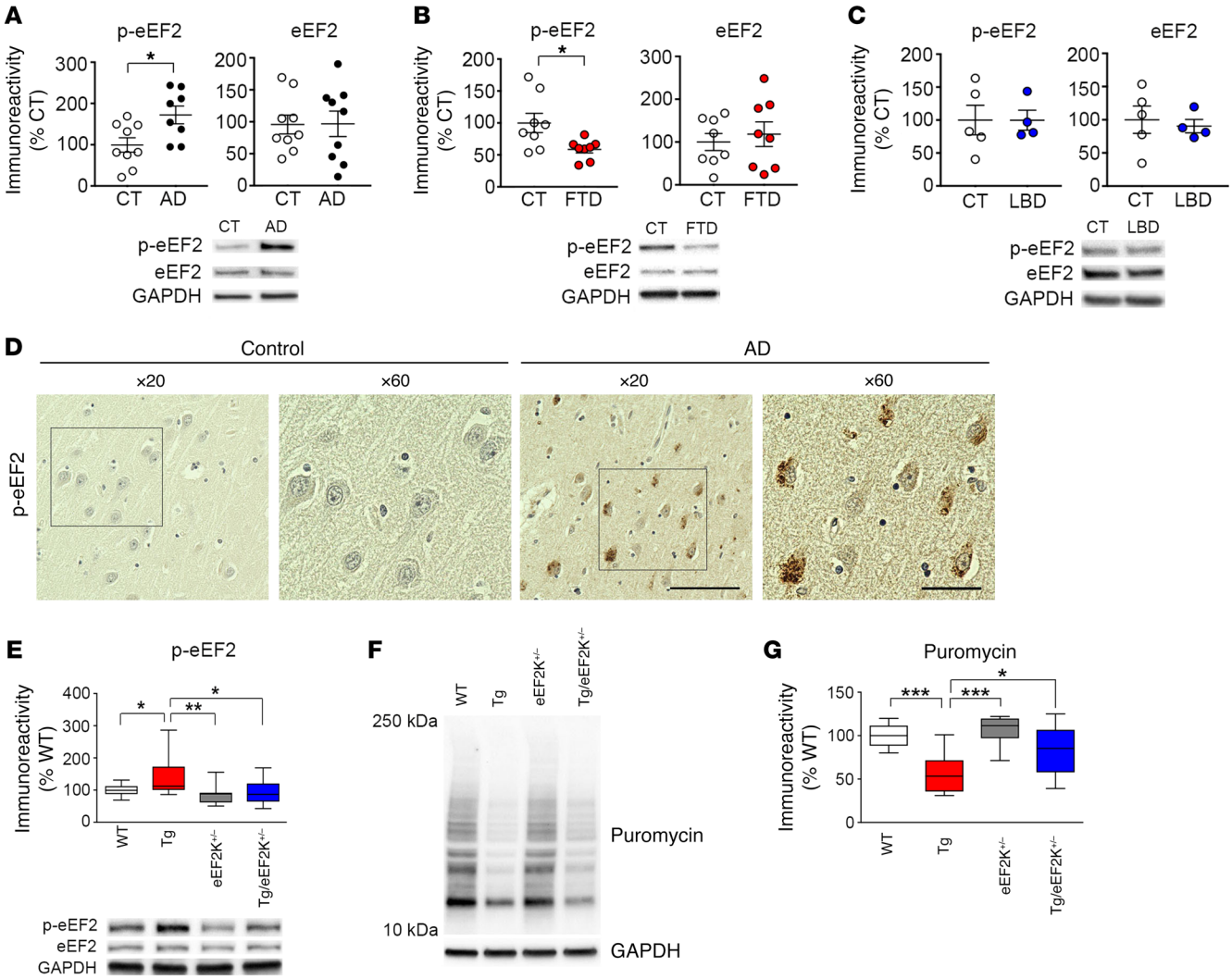

Figure 1. Hyperphosphorylation of eEF2 in the AD hippocampus. (**A**) Postmortem human hippocampal lysates from AD patients exhibit increased eEF2 phosphorylation compared with those of age-matched controls (CT). $n = 9$. $^*P < 0.05$, unpaired t test. (**B**) Human postmortem hippocampal tissue from FTD patients shows decreased eEF2 phosphorylation compared with that of healthy controls. Controls, $n = 8$; FTD, $n = 5$. $^{**}P < 0.01$, unpaired t test. (**C**) eEF2 phosphorylation is not affected in hippocampal tissue from LBD patients ($n = 4$) compared with that of age-matched controls. $n = 5$. $P = 0.99$, unpaired t test. Error bars for human patient data indicate ± SEM. (**D**) Representative images demonstrating hyperphosphorylation of eEF2 in the AD hippocampus. Insets are shown at ×60 magnification. Scale bars: 300 μm (×20); 40 μm (×60). Immunohistochemical experiments were replicated 3 times. (**E**) Genetic reduction of eEF2K corrects eEF2 hyperphosphorylation in hippocampal lysates from Tg19959 AD model mice. $n = 10$. $^*P < 0.05$; $^{**}P < 0.01$, 1-way ANOVA with Tukey's post hoc test. (**F**) Representative images from SUnSET puromycin incorporation assay. Image shows 10–250 kDa range. (**G**) Quantification of de novo protein synthesis via SUnSET assay. WT, $n = 6$ mice; Tg19959, $n = 5$; eEF2K$^{+/-}$, $n = 4$; Tg19959/eEF2K$^{+/-}$, $n = 8$. $^*P < 0.05$; $^{***}P < 0.001$, 1-way ANOVA with Tukey's post hoc test. Box and whisker plots represent the interquartile range, with the line across the box indicating the median. Whiskers show the highest and lowest values detected.

phosphatase 2A (PP2A), the known phosphatase for eEF2, was not affected across the 4 genotypes (Supplemental Figure 1, D–F).

We further investigated the effects of eEF2K reduction on de novo protein synthesis by using surface sensing of translation (SUnSET), a nonradioactive puromycin end-labeling assay (16, 17). Consistent with previous studies, hippocampal de novo protein synthesis (indicated by puromycin labeling) was significantly reduced in Tg19959 mice compared with WT (Figure 1, F and G). In contrast, protein synthesis levels were significantly improved in Tg19959/eEF2K mice compared with Tg19959 mice, which is consistent with suppression of eEF2 phosphorylation (Figure 1, F and G).

eEF2K reduction alleviates cognitive deficits in Tg19959 AD model mice. To determine whether genetic reduction of eEF2K could alleviate AD-associated cognitive impairments, we subjected Tg19959 mice to a series of behavioral tasks. We first performed the open-field (OF) test to assess general locomotor activity and anxiety and did not observe any differences among the 4 genotypes (Supplemental Figure 2, B–D). Next, we used the novel object recognition (NOR) test to assess the animals' working memory ability (18, 19). Both WT and eEF2K$^{+/-}$ mice exhibited preference for the novel object over the familiar object on the test day, as indicated by significantly more interaction with the novel object (Figure 2A). Tg19959 AD model animals, on the other hand,

Table 1. AD patient demographics

Diagnosis	Age (yr)	Sex	PMI (h)	APOE	Braak Stage	CERAD score
No dementia	78	M	6.00	3/3	II	Sparse
No dementia	86	M	3.15	3/3	III	Absent
No dementia	91	F	11.00	4/3	III	Absent
No dementia	92	F	6.00	3/3	III	Rare
No dementia	97	F	10.00	N/A	III	Sparse
No dementia	87	M	4.23	3/3	II	Absent
No dementia	91	M	5.00	3/3	III	Absent
No dementia	94	F	6.00	2/4	III	Sparse
No dementia	95	F	3.05	3/4	III	Absent
No dementia	82	M	5.00	3/2	II	Sparse
AD	82	F	3.20	N/A	VI	Freq
AD	88	M	4.40	4/3	VI	Mod
AD	91	M	7.00	3/4	V	Mod
AD	96	F	4.45	3/3	VI	Freq
AD	98	F	2.30	3/3	IV	Freq
AD	86	M	2.40	3/4	V	Freq
AD	97	F	10.00	3/4	V	Freq
AD	82	F	8.00	3/4	VI	Freq
AD	90	F	5.51	3/3	V	Freq
AD	89	F	3.50	3/3	VI	Mod

APOE, apolipoprotein E allele status; M, male; F, female; Freq, Frequent; Mod, Moderate.

spent roughly equal amounts of time with the familiar and novel objects, indicating a cognitive impairment (Figure 2A). In contrast, Tg19959 mice with reduced eEF2K expression showed performance similar to that of WT mice, spending significantly more time with novel than with familiar objects (Figure 2A).

We next evaluated spatial learning and memory by testing mice on the object location memory (OLM) and Morris water maze (MWM) tasks (17, 20). In the OLM task, both WT and eEF2K$^{+/-}$ mice exhibited normal cognition and spent more time exploring objects at the new location than the old location. Tg19959 mice, however, failed to recognize the relocated object and spent equal amounts of time with both objects, indicating a cognitive deficit (Figure 2B) (20). Notably, Tg19959/eEF2K$^{+/-}$ mice showed a preference for objects in the new location, suggesting normal cognition (Figure 2B). In agreement with these findings, results from the MWM task showed learning and memory impairments in Tg19959 mice that were improved with eEF2K inhibition (Figure 2, C–E). In addition, we tested mice on a visible platform task to assess memory-independent effects associated with eEF2K suppression, such as vision and swimming ability (17). Latency to locate the platform was not significantly different between Tg19959 and Tg19959/eEF2K$^{+/-}$ mice (Supplemental Figure 2I). Taking these data together, suppression of eEF2K alleviated cognitive impairments in Tg19959 mice.

Suppression of eEF2K improves LTP impairments in Tg19959 AD model mice. AD is characterized by synaptic failure (1, 21, 22). We investigated whether eEF2K suppression could prevent AD-associated impairments of long-term potentiation (LTP), a well-characterized form of synaptic plasticity and cellular model for learning and memory (21, 23). While WT and eEF2K$^{+/-}$ mice showed robust, sustained hippocampal LTP over 90 minutes, Tg19959 mice exhibited LTP deficits (Figure 2, F–H). Importantly, genetic reduction of eEF2K attenuated LTP impairments in Tg19959 mice (Figure 2, F–H). To determine whether LTP rescue in the Tg19959/eEF2K$^{+/-}$ mice depended on protein synthesis, we performed LTP experiments in the presence of anisomycin (40 μM), a general mRNA translation inhibitor (2). WT slices treated with anisomycin exhibited LTP failure compared with vehicle-treated slices (Figure 2, I–K). LTP in Tg19959/eEF2K$^{+/-}$ slices was also inhibited by anisomycin treatment, indicating that eEF2K reduction rescued LTP in Tg19959 mice via a protein synthesis–dependent mechanism (Figure 2, I–K). Interestingly, genetic eEF2K depletion did not significantly alter hippocampal LTP in younger Tg19959 mice (4 to 5 months), corroborating recent reports that eEF2K hyperactivity affects AD model animals with age (Supplemental Figure 2, J and K) (15).

We next investigated potential mechanisms through which eEF2K reduction might confer protective effects on Tg19959 mice. We first examined amyloid β (Aβ) pathology and found similar Aβ plaque deposition in the hippocampal and cortical brain areas of Tg19959 and Tg19959/eEF2K$^{+/-}$ mice (Figure 3, A–D). We then used ELISA to determine whether eEF2K reduction affected brain levels of Aβ 1–42 or Aβ 1–40 and found no differences between Tg19959 and Tg19959/eEF2K$^{+/-}$ mice (Figure 3, E and F). Furthermore, eEF2K reduction did not affect the expression of key APP processing enzymes in Tg19959 mice, including β-secretase 1

Table 2. FTD patient demographics

Diagnosis	Age (yr)	Sex	PMI (h)	Braak stage	CERAD score
Control	79	M	4.67	II	None
Control	91	F	3.92	II	Sparse
Control	92	F	5.58	II	Sparse
Control	70	F	4.17	I	Sparse
Control	74	F	4.50	I	Sparse
Control	84	M	3.92	II	None
Control	83	F	3.92	II	None
Control	99	M	8.17	II	Sparse
PSP	75	M	6.50	Tauopathy	Sparse
PSP	74	M	3.00	III	None
PSP	79	M	4.83	I	Freq
PSP	69	F	4.67	Tauopathy	Sparse
PSP	76	M	4.50	Tauopathy	Sparse

PSP, progressive supranuclear palsy.

Table 3. LBD patient demographics

Diagnosis	Age (yr)	Sex	PMI (h)	Braak stage	CERAD score
Control	91	F	3.50	II	Sparse
Control	96	F	6.32	I	Sparse
Control	73	M	4.50	II	None
Control	82	M	5.00	II	Sparse
Control	92	M	6.42	I	None
Neocortical LBD	88	F	4.50	III	None
Neocortical LBD	91	F	4.00	II	Sparse
Neocortical LBD	70	M	8.67	I	Sparse
Neocortical LBD	82	M	5.00	II	Sparse
Neocortical LBD	87	M	8.00	I	Sparse

(BACE1) or γ-secretase subunits (Supplemental Figure 3). Expression of a key Aβ degrading enzyme, neprilysin, was also unaltered with eEF2K inhibition (Supplemental Figure 3C). Together, these results indicate that eEF2K reduction improved long-term memory formation and synaptic plasticity in AD model mice independently of Aβ pathology.

Genetic reduction of eEF2K modulates spine density and morphology in AD model mice. Regulation of dendritic spine morphology is indicative of synaptic integrity and is closely associated with neural plasticity and memory formation (24, 25). Synapse loss correlates robustly with memory impairments in human AD patients and AD animal models (23, 26). Furthermore, de novo protein synthesis can affect spine density, morphology, and synapse strength (5, 27). Using the rapid Golgi-Cox staining protocol (28), we assessed spine density in apical hippocampal dendrites of area CA1 stratum radiatum. Overall dendritic spine density in Tg19959 AD mice was significantly lower compared with that in WT controls and was restored by genetic reduction of eEF2K (Figure 4, A and B). We further analyzed changes in spine morphology based on published guidelines (Supplemental Figure 4) (28). We found that the density of "mature" spines (mushroom, stubby, branched) in Tg19955 mice was decreased compared with that in WT controls. Notably, mature spine morphology in Tg19959/eEF2K$^{+/-}$ mice was restored to WT levels (Figure 4C). No differences were observed for overall "immature" spines (thin and filopodial) across all groups (Figure 4D). Of note, the density of filopodial spines was significantly increased in Tg19959 mice; this was blunted by eEF2K suppression (Supplemental Figure 4F). Furthermore, we used transmission electron microscopy (TEM) to examine postsynaptic densities (PSDs), which are located at the heads of spines and critical for synaptic function (24, 29). Ultrastructural analysis of hippocampal area CA1 revealed decreased PSD density in Tg19959 mice, which was restored to WT levels by suppression of eEF2K (Figure 4, E and F). Taking these data together, genetic suppression of eEF2K prevented defects in hippocampal spine density/morphology and PSD formation in Tg19959 AD model mice. These data are consistent with the results from our behavioral and electrophysiological studies (Figure 2).

Genetic reduction of eEF2K upregulates protein synthesis capacity in AD model mice. We showed that resistance to LTP failure in Tg19959/eEF2K$^{+/-}$ hippocampal slices depended on de novo protein synthesis (Figure 2, I–K). Protein incorporation assays and polysome profiling both show reduced translational capacity in the brains of human AD patients (7, 8). Polyribosomes are clusters of ribosomes engaged in active, ongoing translation; increased polyribosome count implies greater translational capacity and has been associated with synaptic plasticity and memory formation (30, 31). We utilized transmission EM (TEM) to investigate whether suppression of eEF2 phosphorylation via eEF2K reduction affected polyribosomes in area CA1 of the hippocampus. Compared with WT, Tg19959 mice exhibited fewer dendritic polyribosomes, indicating impaired mRNA translation. Notably, genetic reduction of eEF2K improved dendritic polyribosome deficiency in Tg19959 mice (Figure 5, A and B). Interestingly, polyribosome assembly was unaltered in eEF2K$^{+/-}$ mice (Figure 5, A and B). These findings are consistent with our SUnSET data (Figure 1, F and G), suggesting improvement of de novo protein synthesis in AD mice with eEF2K suppression. We further performed mass spectrometry–based (MS-based) proteomic experiments to assess alterations of protein profiling. In brief, proteins upregulated by genetic eEF2K reduction were central to synaptic function, calcium buffering, mitochondrial function, and ATP generation (Figure 5C and Table 4). Reduced eEF2K expression downregulated certain cytoskeletal proteins, calcium signaling, plasma membrane dynamics, RNA binding, protein folding, and nitric oxide generation (Figure 5D and Table 5). Ten proteins in total were significantly changed in Tg19959 compared with WT mice and normalized with eEF2K reduction. These included proteins involved in Ca^{2+} signaling, cytoskeletal dynamics, mitochondrial function and ATP biosynthesis, and synaptic function (Tables 4 and 5).

Suppression of eEF2K corrects defects in APP/PS1 AD model mice. We further replicated our findings in APP/PS1 mice, another established rodent model of AD (32). We crossed APP/PS1 mice with heterozygous *Eef2k*$^{+/-}$ mice to generate WT, APP/PS1, eEF2K$^{+/-}$ knockdown, and APP/PS1/eEF2K$^{+/-}$ double-mutant littermates. Like Tg19959 mice, the APP/PS1 animals exhibited hippocampal eEF2 hyperphosphorylation that was corrected by eEF2K reduction independently of total eEF2 levels (Figure 6, A and B, and Supplemental Figure 5A).

To validate the effects of eEF2K knockdown on hippocampal-dependent long-term memory formation in AD model mice, 10- to 12-month-old male and female WT, APP/PS1, eEF2K$^{+/-}$, and APP/PS1/eEF2K$^{+/-}$ mice were subjected to the NOR and OLM tasks. Performance of APP/PS1 mice was impaired in both paradigms. In the NOR task, APP/PS1 mice failed to discriminate object novelty (Figure 6C). Similarly, APP/PS1 mice did not distinguish between object locations in the OLM task (Figure 6D). In contrast, APP/PS1/eEF2K$^{+/-}$ mice exhibited normal cognition in both behavioral paradigms (Figure 6, C and D). We further evaluated synaptic plasticity in these animals by inducing LTP in hippocampal slices. APP/PS1 slices exhibited LTP failure that was alleviated with genetic eEF2K knockdown (Figure 6, E and F). Finally, brain levels of both Aβ 1–42 and 1–40 peptides were not significantly altered in APP/PS1 mice with genetic reduction of eEF2K (Figure 6, G and H). More-

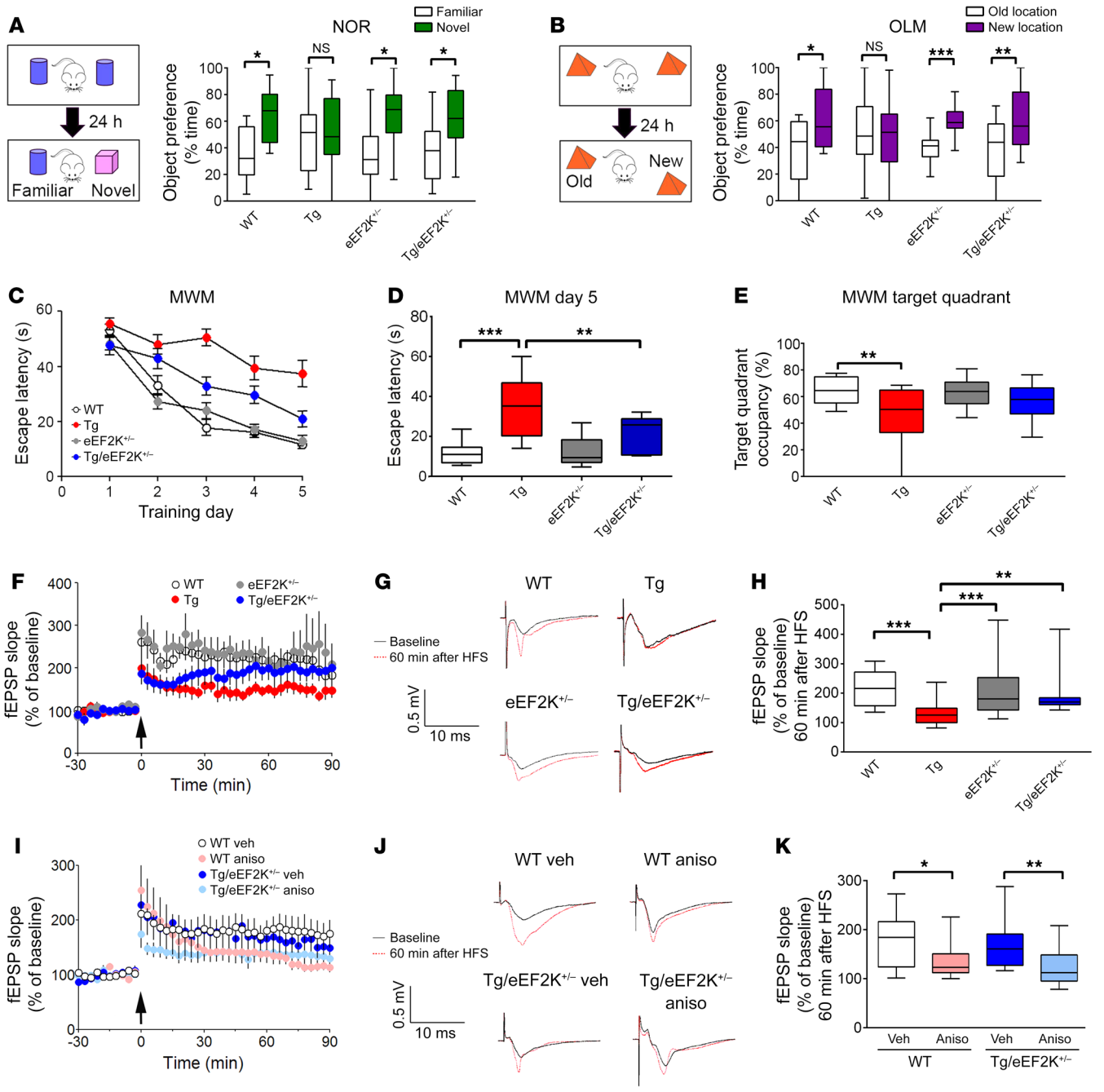

Figure 2. Genetic reduction of eEF2K restores cognitive dysfunction and LTP impairments in Tg19959 AD model mice. (**A**) Novel object recognition (NOR) paradigm and object preference for familiar and novel object. (WT, $n = 11$; Tg19959, $n = 14$; eEF2K$^{+/-}$, $n = 14$; Tg19959/eEF2K$^{+/-}$, $n = 11$. $^{*}P < 0.05$, paired t test). (**B**) OLM task and object preference for familiar and new locations (WT, $n = 10$; Tg19959, $n = 11$; eEF2K$^{+/-}$, $n = 12$; Tg19959/eEF2K$^{+/-}$, $n = 10$. $^{*}P < 0.05$; $^{**}P < 0.01$; $^{***}P < 0.001$, paired t test). (**C**) Escape latency in MWM. Tg19959 ($n = 12$) had significantly longer latency to platform than WT ($n = 14$; $P < 0.001$), eEF2K$^{+/-}$ ($n = 15$; $P < 0.001$), and Tg19959/eEF2K$^{+/-}$. $n = 10$. $P < 0.05$, 1-way repeated measures ANOVA with Tukey's post hoc tests. (**D**) Escape latency on day 5 of MWM training. $^{**}P < 0.01$; $^{***}P < 0.001$, 1-way ANOVA with Tukey's post hoc test. (**E**) Percentage of time in target quadrant during MWM probe trial. $^{**}P < 0.01$, 1-way ANOVA with Tukey's post hoc test. (**F**) Hippocampal LTP in WT ($n = 12$ slices), Tg19959 ($n = 9$), eEF2K$^{+/-}$ ($n = 9$), and Tg19959/eEF2K$^{+/-}$ ($n = 9$) mice. Arrow indicates HFS. Tg19959 slices had significantly impaired LTP compared with WT ($P < 0.0001$), eEF2K$^{+/-}$ ($P < 0.0001$), and Tg19959/eEF2K$^{+/-}$ ($P < 0.01$) slices (1-way repeated measures ANOVA with Tukey's post hoc tests). (**G**) Representative traces before and after HFS. (**H**) fEPSP slope 60 minutes after HFS. $^{**}P < 0.01$; $^{***}P < 0.001$, 1-way ANOVA with Tukey's post hoc test. (**I**) WT and Tg19959/eEF2K$^{+/-}$ slices were treated with vehicle (DMSO; WT, $n = 7$ slices; Tg19959/eEF2K$^{+/-}$, $n = 10$) or the protein synthesis inhibitor anisomycin (40 μM; WT, $n = 7$; Tg19959/eEF2K$^{+/-}$, $n = 17$) and stimulated with HFS to induce LTP. Tg19959/eEF2K$^{+/-}$ slices exposed to anisomycin had significantly impaired LTP compared with vehicle slices. $P < 0.0001$, 1-way repeated measures ANOVA with Tukey's post hoc tests. (**J**) Representative traces before and after HFS. (**K**) fEPSP slope 60 minutes after HFS. $^{*}P < 0.05$; $^{**}P < 0.01$, 1-way ANOVA with Tukey's post hoc test.

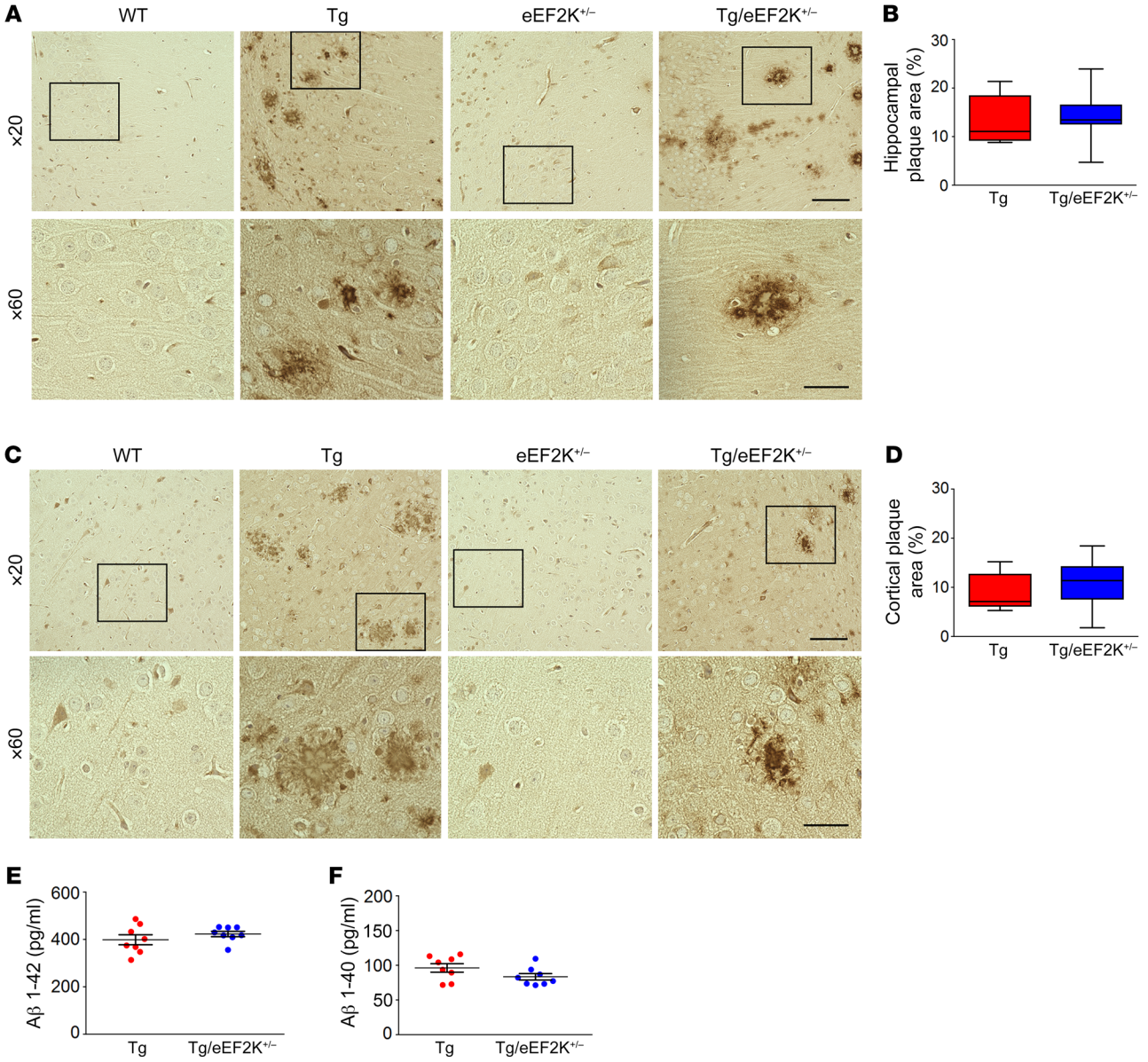

Figure 3. Amyloid plaque deposition in Tg19959 AD model mice is not affected by genetic reduction of eEF2K. (**A**) Representative images of hippocampal plaque deposition in WT, Tg19959, eEF2K$^{+/-}$, and Tg19959/eEF2K$^{+/-}$ mice. Insets are shown at ×60 magnification. Scale bars: 300 μm (×20); 40 μm (×60). (**B**) Percentage of hippocampal area covered in amyloid plaques in Tg19959 (n = 9 sections) and Tg19959/eEF2K$^{+/-}$ mice (n = 10). P = 0.68, unpaired t test. (**C**) Representative images of somatosensory cortical plaque deposition in WT, Tg19959, eEF2K$^{+/-}$, and Tg19959/eEF2K$^{+/-}$ mice. Insets are shown at ×60 magnification. Scale bars: 300 μm (×20); 40 μm (×60). (**D**) Percentage of cortical area covered by amyloid plaques in Tg19959 and Tg19959/eEF2K$^{+/-}$ mice. P = 0.33, unpaired t test. Box and whisker plots represent the interquartile range, with the line across the box indicating the median. Whiskers show the highest and lowest values detected. (**E**) ELISA showed no differences in levels of Aβ 1–42 or Aβ 1–40 oligomers (**F**) in Tg19959 and Tg19959/eEF2K$^{+/-}$ forebrain tissue. n = 8. P = 0.32 for Aβ 1-42; P = 0.11 for Aβ 1-40, unpaired t test. ELISAs were performed in triplicate. Error bars represent ± SEM.

over, brain levels of p-tau were similar between APP/PS1 and APP/PS1/eEF2K$^{+/-}$ mice (Supplemental Figure 5F). These findings are consistent with the results from the Tg19959 mouse experiments described above, indicating that genetic suppression of eEF2K activity, and thus eEF2 phosphorylation, prevents AD-associated cognitive impairments and synaptic plasticity failure.

Discussion

Present disease-modifying strategies in AD clinical trials have met with limited success, and it is urgent to identify alternative therapeutic avenues based on solid mechanistic studies. Here, we report that genetic reduction of eEF2K alleviated memory impairments and synaptic failure in 2 separate lines of AD model mice, raising the possibility that targeting the eEF2K/eEF2 signaling pathway could protect against AD and other cognitive syndromes associated with dysregulated protein synthesis. Our findings are consistent with recent studies showing AD-associated hyperactivity of AMPK, a molecular energy sensor that activates eEF2K via phosphorylation in response to low energy states (14, 33, 34). AD is characterized by oxidative stress and energy metabolism defi-

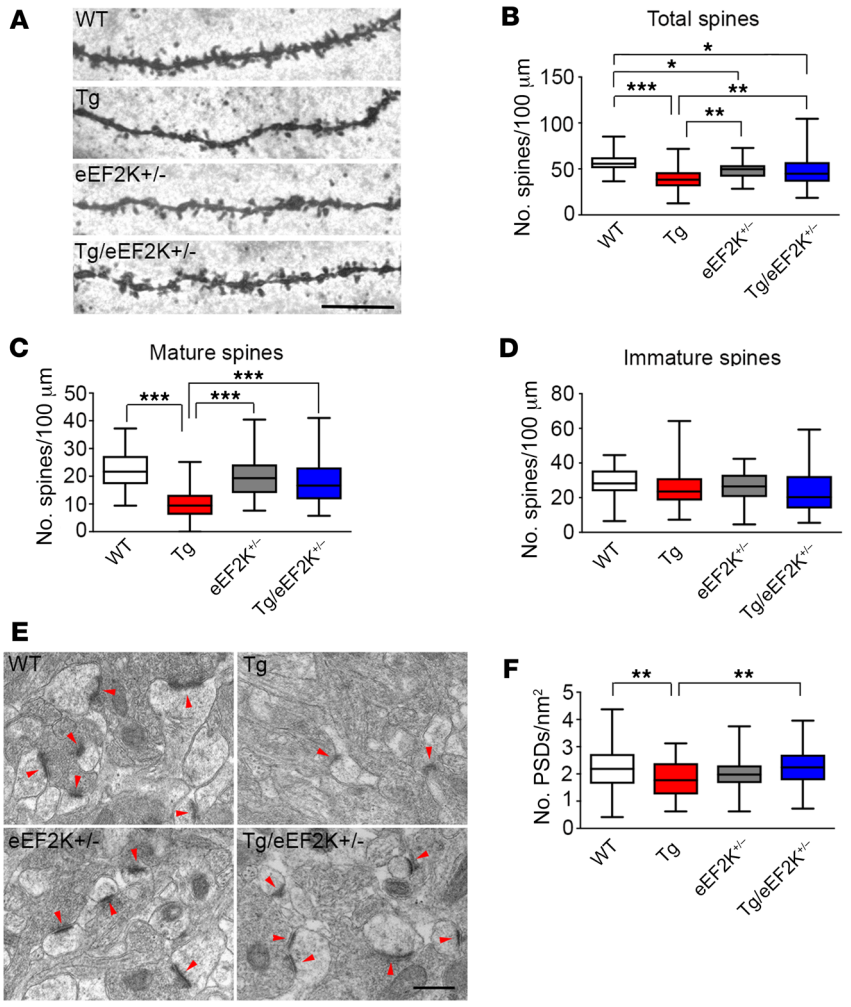

Figure 4. Genetic reduction of eEF2K restores spine density in hippocampus from Tg19959 mice. (**A**) Representative images from Golgi-Cox stain of area CA1 dendritic spines. Original magnification, ×100. Scale bar: 12 μm. (**B**) Total CA1 spine density per 100 μm. WT, n = 34 dendrites; Tg19559, n = 58; eEF2K$^{+/-}$, n = 40; Tg19959/eEF2K$^{+/-}$, n = 50. (**C**) Mature spine density per 100 μm. Branched and mushroom type spines were classified as mature. (**D**) Immature spine density per 100 μm. Thin and filopodial spines were classified as immature. (**E**) Representative TEM images for CA1 PSDs. n = 3 mice per genotype. Original magnification, ×11,000. Scale bar: 500 nm. (**F**) Number of PSDs per μm^2. *P < 0.05; **P < 0.01; ***P < 0.001, 1-way ANOVA with Tukey's post hoc test. Box and whisker plots represent the interquartile range, with the line across the box indicating the median. Whiskers show the highest and lowest values detected.

ciency (21, 35, 36). Phosphorylation of eEF2 by eEF2K (controlled by AMPK) inhibits general protein synthesis, which is a protective strategy under physiological conditions for cells to cope with stress, since decreased mRNA translation helps cells conserve energy and enhance the expression of stress-related proteins (37, 38). It was also reported that eEF2K activation promotes survival of tumor cells under conditions of nutrient deprivation (39). Nevertheless, severe and prolonged cellular stress under pathological conditions, such as AD, results in long-term and irreversible mRNA translation suppression, which is detrimental because de novo protein synthesis is critical for the maintenance of memory and synaptic plasticity (27, 40).

Protein synthesis takes place in 3 phases: initiation, elongation, and termination. Much attention has been given to the initiation process, which is usually considered the rate-limiting step during de novo protein synthesis (41). However, low cellular mRNA translational capacity in neuronal dendrites would require upregulation of both initiation and elongation processes to meet the substantial need of new protein synthesis associated with maintenance of memory and synaptic plasticity (27). The mammalian (mechanistic) target of rapamycin complex 1 (mTORC1) and eukaryotic initiation factor 2 (eIF2) signaling cascades are critical for regulation of translation initiation in protein synthesis–dependent forms of memory and synaptic plasticity (42, 43). mTORC1 also controls translation elongation by inhibiting eEF2K and thus eEF2 phosphorylation either directly or through its downstream effector S6 kinase 1 (S6K1) (12). Further, we previously reported increased phosphorylation of the α subunit of eIF2 (eIF2α) in AD brains (17). Suppression of eIF2α phosphorylation corrected AD-associated cognitive and synaptic plasticity defects (17), indicating a crucial role of translation initiation dysregulation in AD pathogenesis. Mounting evidence suggests an important role for elongation regulation in cognition, with recent studies linking dysregulation of elongation factors with AD pathophysiology (15, 44–47). Of note, a recent study showed a connection between eIF2 signaling and eEF2 phosphorylation in neurons (48). While additional studies are warranted to evaluate AD-associated dysregulation of initiation and elongation separately, there is evidence for crosstalk between these 2 phases of translation via eIF2 and eEF2. How this relationship is affected in AD remains to be elucidated. Unlike initiation, however, elongation may offer more promising therapeutic strategies for dementia treatment. The only known substrate for eEF2K is eEF2, and this specificity makes it an attractive target for AD therapy in avoiding off-target effects. Further, there are several available selective eEF2K antagonists, and future studies are important to determine whether these inhibitors are effective in alleviating cognition defects in AD (12, 49).

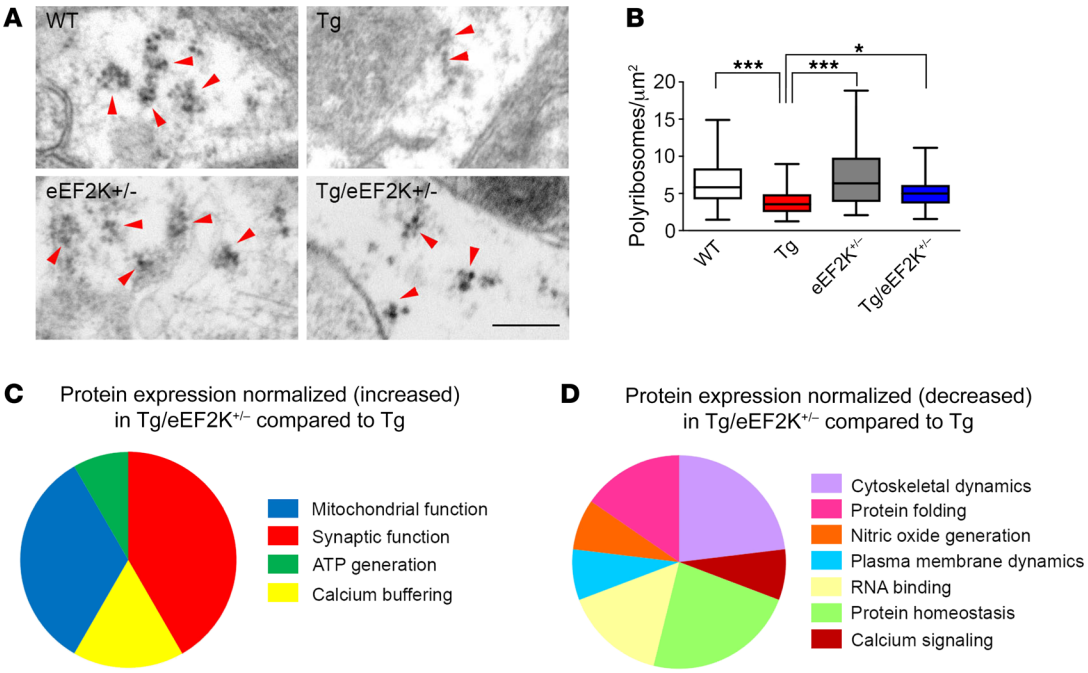

Figure 5. Suppression of eEF2K enhances translation in hippocampus from Tg19959 mice. (**A**) Representative TEM images for CA1 polyribosomes. Arrows indicate polyribosomes. n = 3 mice per genotype. Original magnification, ×11,000. Scale bar: 500 nm. (**B**) Number of polyribosomes per μm². $^*P < 0.05$; $^{***}P < 0.001$, 1-way ANOVA with Tukey's post hoc test. Box and whisker plots represent the interquartile range, with the line across the box indicating the median. Whiskers show the highest and lowest values detected. (**C**) Functional classification of proteins upregulated in hippocampus from Tg19959/eEF2K$^{+/-}$ compared with Tg19959 mice by MS analysis. n = 3 mice per genotype. (**D**) Functional classifications of proteins downregulated in Tg19959/eEF2K$^{+/-}$ compared with Tg19959 hippocampi.

The eEF2/eEF2K signaling pathway is implicated in memory formation and synaptic function. A recent study showed that synaptic activity could modulate spine morphology via eEF2K activity. Repression of eEF2K activity impaired spine formation and dendritic BDNF release (50). This work seemingly contradicts our own, as we found eEF2K knockdown enhanced dendritic spine density and maturity in Tg19959 AD model mice (Figure 4). There are a number of important differences between the 2 studies, including the model system (cultured neurons from rats vs. aged mice) and approaches (siRNA vs. knockout mice). Interestingly, we did observe significantly fewer stubby spines in the heterozygous eEF2K$^{+/-}$ dendrites compared with WT (Supplemental Figure 4D). Multiple lines of evidence indicate that the eEF2/eEF2K pathway serves as a molecular sensor of synaptic stimulation that modulates the homeostatic conditions of the neuron (51). Our findings demonstrate the importance of this homeostatic balance, revealing the detrimental effects of either overactivation or underactivation of eEF2K on synapse morphology.

eEF2K is also known as Ca^{2+}/calmodulin-dependent kinase III (CaMKIII) because it is activated by Ca^{2+}/calmodulin (12, 52). Aberrant Ca^{2+} homeostasis is linked to AD pathogenesis (53, 54). Extracellular influx of Ca^{2+} via *N*-methyl-D-aspartate receptors (NMDARs) and/or release of Ca^{2+} from intracellular stores under endoplasmic reticulum stress in AD likely drives a number of pathological mechanisms, including eEF2K overactivation and subsequent eEF2 hyperphosphorylation (53). Moreover, our proteomics study showed that eEF2K reduction in AD model mice restored protein levels of calbindin, a Ca^{2+}-buffering molecule, and reduced levels of the L-type Ca^{2+} channel modulator NIPSNAP2 (55, 56). These results suggest a feedback loop between Ca^{2+} levels and eEF2K/eEF2 signaling, providing an additional mechanistic explanation for improvements of AD-associated cognitive and plasticity impairments by eEF2K suppression.

It is worth mentioning that hippocampal eEF2K phosphorylation was increased in AD, but not in FTD or LBD, brain samples (Figure 1). AD cases in this study were characterized by high levels of hippocampal phosphorylated τ (neurofibrillary tangles) and Aβ (plaques). FTD cases (all patients reported here were diagnosed

Table 4. Top proteins increased in Tg/eEF2K$^{+/-}$ brains compared with Tg19959

Ascension ID	Protein name	Function	Fold change
P12658	Calbindin	Calcium buffering	1.72
P18760	Cofilin1	Synaptic function	1.11
Q6Q477	Plasma membrane calcium transporting ATPase 4	Calcium buffering	1.29
Q80TZ3	Putative tyrosin-protein phosphatase auxilin	Synaptic function	1.30
Q9D880	Mitochondrial import inner membrane translocase subunit TIM50	Mitochondrial function	1.57
Q9QYX7	Protein piccolo	Synaptic function	1.20

Table 5. Top proteins decreased in Tg/eEF2K$^{+/-}$ brain compared with Tg19959

Ascension ID	Protein name	Function	Fold change
Ascension ID	Protein name	Function	Fold change
O55126	NIPSNAP2	Calcium signaling	0.81
P52196	Thiosulfate sulfurtransferase	RNA binding	0.75
Q9CWS0	N(G),N(G)-dimethylarginine dimethylaminohydrolase	Nitric oxide generation	0.73
Q9QYX7	Proteasome subunit α type 6	Protein homeostasis	0.65

with progressive supranuclear palsy) typically have significant hippocampal τ phosphorylation (p-tau), while LBD cases are burdened by hippocampal α-synuclein and lack substantial levels of p-tau (57, 58). Moreover, both FTD and LBD cases lack significant hippocampal Aβ deposition (57, 58). Our findings suggests that eEF2 hyperphosphorylation may be specific to AD-related pathological processes, such as Aβ or AD-type p-tau, and not related to frontotemporal lobar degeneration-tau (FTLD-tau), α-synuclein, or nonspecific neurodegenerative disease processes that span a diverse array of conditions. Interestingly, we did observe a significant decrease in hippocampal eEF2 phosphorylation in FTD patients (Figure 1B). Future studies are needed to evaluate the specificity of eEF2 hyperphosphorylation to the pathologic changes in AD and other dementia syndromes.

In summary, our work demonstrates that eEF2K reduction rescues long-term memory and synaptic plasticity deficits in AD model mice. Genetic reduction of eEF2K influenced memory and plasticity-related mechanisms, including spine density, and upregulation of de novo protein synthesis. Thus, the eEF2/eEF2K pathway may be a potential therapeutic target for future AD interventions.

Methods

Postmortem tissue samples. All postmortem human tissue was obtained from the University of Washington School of Medicine Brain Bank. Diagnoses were based on cognitive testing, postmortem Braak staging (AD stages V–VI) stage, and Consortium to Establish a Registry for Alzheimer's Disease (CERAD) scores (59, 60). Studies were performed using hippocampal tissue from male and female patients clinically diagnosed with AD (n = 9) and age-matched controls (n = 9). Patient information is presented in Table 1. Mean age of death was 89.6 years. Postmortem interval (PMI) ranged between 2 and 10 hours, with a mean of 5.3 hours. For hippocampal tissue from FTD patients (n = 5) and age-matched controls (n = 8), mean age of death was 80.4 years, with a PMI between 3 and 9 hours and an average of 4.8 hours (Table 2). For hippocampal tissue from LBD patients (n = 5) and age-matched controls (n = 5), mean age of death was 85.2 years, with a PMI between 3.5 and 9 hours and an average of 5.6 hours (Table 3).

Mice. All mice were housed at the Wake Forest School of Medicine barrier facility under the supervision of the Animal Research Program. Mice adhered to a 12-hour light/12-hour dark cycle, with regular feeding, cage cleaning, and 24-hour food and water access. Both male and female mice were used for experimentation. Homozygous *Eef2k*$^{-/-}$ mice and Tg19959 AD model mice were generated as described before (61–63). Briefly, Tg19959 mice overexpress mutant human amyloid precursor proteins (APP KM670/671NL, V717F) (62). Breeders of Tg19959 AD model mice were a gift from George Carlson of McLaughlin Research Institute (Great Falls, Montana, USA). Tg19959 and *eEF2K*$^{+/-}$ mice were crossbred to generate 4 littermate groups (mixed C57BL/6 and 129S background): WT, Tg19959, eEF2K$^{+/-}$, and Tg/eEF2K$^{+/-}$ mice. APP/PS1 mice were purchased from the Jackson Laboratory and expressed human transgenes for APP (KM670/671NL) and presenilin-1 (PSEN1 L166P) (32). APP/PS1 mice were crossbred with *Eef2k*$^{+/-}$ mice to generate littermate groups (C57BL/6): WT, APP/PS1, eEF2K$^{+/-}$, and APP/PS1/eEF2K$^{+/-}$ double-mutant mice (APP/eEF2K$^{+/-}$). All genotyping was determined by PCR. Tg19959 cohorts underwent all experimental protocols at 6 to 9 months of age, while APP/PS1 cohorts were evaluated at 10 to 12 months of age (32, 62). To assess hippocampal synaptic plasticity at a younger age, Tg19959 cohorts were subjected to electrophysiological experiments for measurement of LTP at 4 to 5 months of age.

OF assay. Mice were handled for at least 5 days prior to behavioral testing and habituated to the testing facility for an hour prior to experimentation. Animals were placed in an opaque plastic OF chamber (40 cm × 40 cm × 40cm) and allowed to explore for 15 minutes. Time spent in the center and periphery of the chamber was measured and calculated as a percentage of total time. Distance moved and velocity were measured using EthoVision XT Tracking Software (Noldus Information Technology). Data collection and analysis were performed blinded.

NOR. Mice underwent a 2-day familiarization protocol in which they were placed in an opaque, plastic arena (40 cm × 40 cm × 40 cm) with 2 identical objects and allowed to explore for 5 minutes. Twenty-four hours after familiarization, animals were tested in the arena for 5 minutes with one object replaced with a novel object. All objects were randomly assigned to mice, and placement of novel objects was counterbalanced. Time spent with each object was measured and calculated as a percentage of the total interaction time. Novel object preference of less than 50% indicates memory impairment (18). Time with objects was measured both manually and using EthoVision 7 tracking software. Mice with a total interaction time of less than 10 seconds were excluded from analysis. Data collection and analysis were performed blinded.

OLM task. Mice were habituated to an opaque, plastic chamber (40 cm × 40 cm × 40 cm) with visible spatial cues for 10 minutes. After 24 hours, mice were returned to the chamber with 2 identical objects placed in the arena and allowed to freely explore for 10 minutes. Twenty-four hours later, mice were again returned to the chamber with one object moved to the opposite side of the arena. Objects and changes in object location were randomly determined and counterbalanced. Time spent with each object was measured and calculated as a percentage of the total interaction time. Novel object preference of less than 50% indicates memory impairment (18). Time with objects was measured both manually and using EthoVision XT tracking software. Mice with a total interaction time of less than 10 seconds were excluded from analysis. Data collection and analysis were performed blinded.

MWM. MWM was performed as previously described (17). The paradigm consisted of 4 trials (60-second maximum, 15-minute interval) per day for 5 consecutive days. Escape latency was measured each training day. A probe trial was performed 2 hours following training on the fifth day. The visible platform task consisted of 4 trials per day for 2 consecutive days, with the escape platform marked by a visible cue and moved

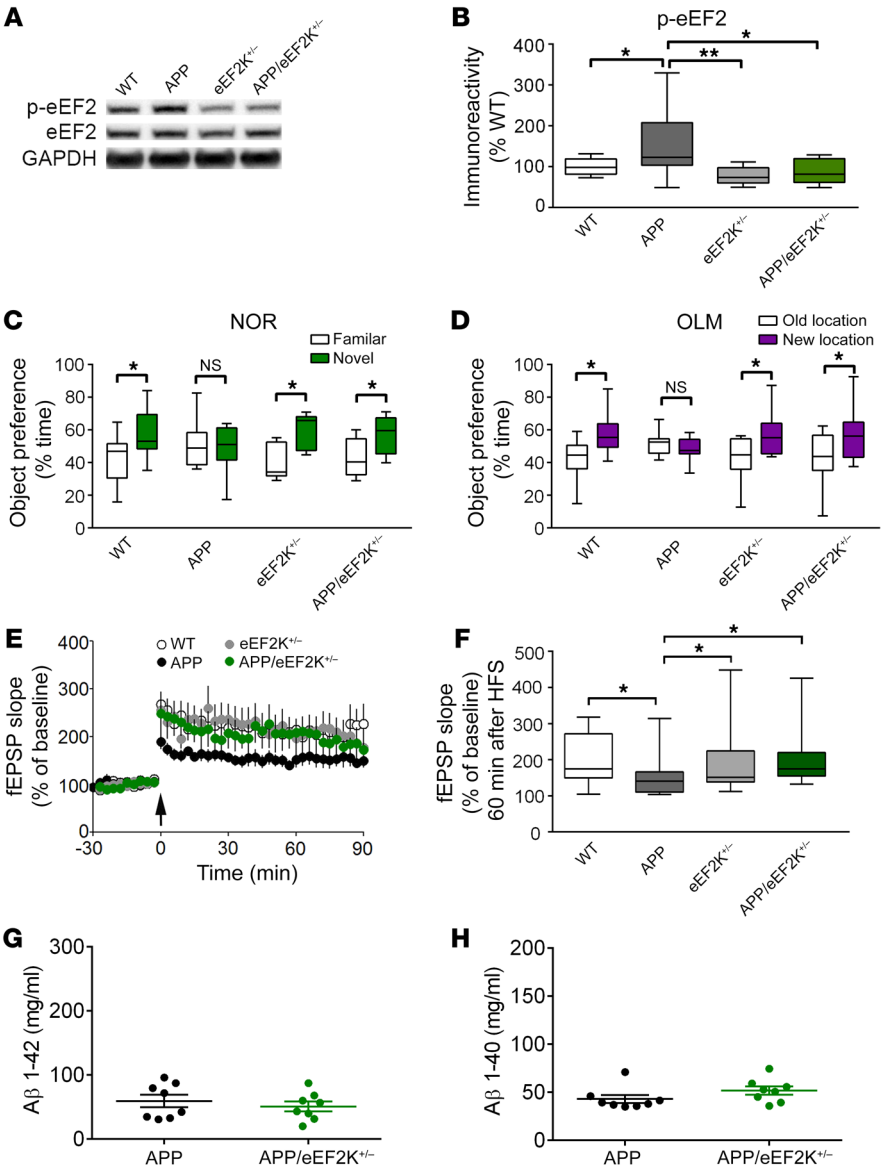

Figure 6. Reduction of eEF2K rescued memory and synaptic plasticity failure in APP/PS1 AD model mice. (**A**) Representative images showing decreased eEF2 phosphorylation in APP/PS1 AD model mice with genetic reduction of eEF2K. (**B**) Quantification of results shown in **A**. WT, $n = 9$; APP/PS1, $n = 10$; eEF2K$^{+/-}$, $n = 9$; APP/PS1/eEF2K$^{+/-}$, $n = 10$. $^*P < 0.05$; $^{**}P < 0.01$, 1-way ANOVA with Tukey's post hoc tests. (**C**) Object preference for familiar or novel objects in NOR paradigm. WT, $n = 12$; APP/PS1, $n = 13$; eEF2K$^{+/-}$, $n = 10$; APP/PS1/eEF2K$^{+/-}$, $n = 13$. $^*P < 0.05$, paired t test. (**D**) Object preference in familiar or new location in OLM task. $^*P < 0.05$, paired t test. (**E**) Acute hippocampal slices were stimulated with HFS to induce LTP at the CA3-CA1 synapse. WT, $n = 11$; APP/PS1, $n = 12$; eEF2K$^{+/-}$, $n = 7$; APP/PS1/eEF2K$^{+/-}$, $n = 9$. APP/PS1 slices exhibited significantly impaired LTP compared with WT ($P < 0.0001$), eEF2K$^{+/-}$ ($P < 0.0001$), and APP/PS1/eEF2K$^{+/-}$ ($P < 0.0001$) slices. One-way repeated measures ANOVA with Tukey's post hoc tests. (**F**) fEPSP slope 60 minutes after HFS. $^*P < 0.05$, 1-way ANOVA with Tukey's post hoc tests. (**G**) ELISA showed no differences in levels of Aβ 1–42 or Aβ 1–40 oligomers (**H**) in APP/PS1 and APP/PS1/eEF2K$^{+/-}$ forebrain tissue. $n = 8$. $P = 0.49$ for Aβ 1-42; $P = 0.17$ for Aβ 1-40, unpaired t test. ELISAs were performed in triplicate. Box and whisker plots represent the interquartile range, with the line across the box indicating the median. Whiskers show the highest and lowest values detected. Scatter plots are shown with mean ± SEM.

randomly among 4 locations. Trajectories, time spent in each maze quadrant, velocity, and distance moved were recorded using EthoVision XT software. Data collection and analysis were performed blinded.

Hippocampal slice preparation and electrophysiology. Acute 400 μm transverse hippocampal slices were prepared using a Leica VT1200S vibratome, as described previously (45). Slices were maintained before experimentation at room temperature for at least 2 hours in artificial cerebrospinal fluid (ACSF) containing the following: 118 mM NaCl, 3.5 mM KCl, 2.5 mM $CaCl_2$, 1.3 mM $MgSO_4$, 1.25 mM NaH_2PO_4, 5.0 mM $NaHCO_3$, and 15 g mM lucose, bubbled with 95% O_2/5% CO_2. For electrophysiology, slices were maintained at 32°C. Monophasic, constant-current stimuli (100 μs) were delivered with a bipolar silver electrode placed in the stratum radiatum of area CA3. Field excitatory postsynaptic potentials (fEPSPs) were recorded using a glass microelectrode from the stratum radiatum of area CA1. LTP was induced using high-frequency stimulation (HFS) consisting of two 1-second 100 Hz trains separated by 60 seconds, each delivered at 70%–80% of the intensity that evoked spiked fEPSPs. Data collection and analysis were not performed blinded.

Western blots for postmortem human tissue. Hippocampal tissue from AD, FTD, and LBD patients and their respective age-matched controls was sonicated as previously described (45). Samples containing equal amounts of protein lysate were loaded on 4%–12% Tris-glycine SDS-PAGE gels (Bio-Rad, catalog 4561023) for standard gel electrophoresis. Following transfer, nitrocellulose membranes were blocked for 10 minutes in SuperBlock TBS Blocking Buffer (Thermo Fisher Scientific, catalog 37535). All primary and secondary antibodies were diluted in 5% milk/TBST. Blots were probed with primary antibodies for phospho-eEF2 (1:1000; Cell Signaling Technology, catalog 2331), eEF2 (1:1000, Cell Signaling Technology, catalog 2332), and GAPDH (1:10,000, Cell Signaling Technology, catalog 5174). Proteins were visualized using the ChemiDoc Imaging System (Bio-Rad). Densitometric analysis was performed using ImageJ software (NIH).

Western blots for mouse tissue. Mouse hippocampal tissue was flash-frozen on dry ice and sonicated as previously described in lysis buffer with protease and phosphatase inhibitors (45). Samples containing equal amounts of protein lysate were loaded on 4%–12% Tris-glycine SDS-PAGE (Bio-Rad) gels for standard gel electropho-

resis. Following transfer, nitrocellulose membranes were blocked for 10 minutes in SuperBlock TBS Blocking Buffer (Thermo Fisher Scientific). All primary and secondary antibodies were diluted in 5% milk/TBST or 5% BSA/TBST. Blots were probed with primary antibodies for phospho-eEF2 (1:1000; Cell Signaling Technology, catalog 2331), eEF2 (1:1000, Cell Signaling Technology, catalog 2332), PP2AA (1:1000; Cell Signaling Technology, catalog 2041), PP2AB (1:1000; Cell Signaling Technology, catalog 4953), PP2AC (1:1000; Cell Signaling Technology, catalog 2038), BACE1 (1:1000; Cell Signaling Technology, catalog 5606), CD10/neprilysin (1:1000; Santa Cruz Biotechnology, catalog sc-46656), nicastrin (1:1000; Cell Signaling Technology, catalog 9447), PS1 (1:1000; Cell Signaling Technology, catalog 5643), PS2 (1:1000; Cell Signaling Technology, catalog 9979), PEN2 (1:1000; Cell Signaling Technology, catalog 8502), phospho-tau (Ser416) (1:1000; Cell Signaling Technology, catalog 15013), and GAPDH (1:10,000, Cell Signaling Technology, catalog 5174). Proteins were visualized using the ChemiDoc Imaging System (Bio-Rad). Densitometric analysis was performed using Bio-Rad ImageLab and ImageJ software.

Golgi-Cox stain. Brains were processed using the FD Rapid GolgiStain Kit in accordance with the manufacturer's instructions (FD Neurotechnologies, catalog PK401). Transverse sections (100 μm) were made using a Leica VT1200S vibratome and mounted onto gelatin-coated slides. Development was performed according to kit instructions. Sections were dehydrated through a graded ethanol series and cleared in xylene. Slides were coverslipped with Vecta-Mount Permanent Mounting Medium (Vector Labs, catalog H-5000) and imaged at ×100 on a Keyence BZ-X710 microscope. Area CA1 stratum radiatum apical dendrites were quantified. For spine analysis, images were blinded, and spines were manually counted and sorted as previously described (28).

TEM. Brains were removed, and 1 mm thick transverse slices were cut using a Leica VT1200S vibratome. The CA1 was dissected and immediately fixed in 2.5% glutaraldehyde/1% paraformaldehyde in 0.1M Millonig's phosphate buffer (pH 7.3) overnight. The samples were washed in buffer and post-fixed with 1% osmium tetroxide in phosphate buffer for 1 hour. After washing, samples were dehydrated through a graded series of ethanol solutions. For preparation of resin infiltration, the samples were incubated in propylene oxide for two 15-minute changes. Finally, the samples were gradually infiltrated with 1:1, 1:2, and pure solutions of Spurr's resin and cured in a 70°C oven overnight. Sections of 90 nm were obtained with a Reichert-Jung Ultracut E ultramicrotome, stained with lead citrate and uranyl acetate, and viewed with a Tecnai Spirit transmission electron microscope operating at 80 kV (FEI Co.). Images were obtained with a 2Vu CCD camera (Advanced Microscopy Techniques) at ×11,000. Analysis for PSDs and polyribosomes was performed as previously described (30, 31). Imaging and analysis were done by investigators blinded to animal groups.

SUnSET assay. Acute 400 μm transverse hippocampal slices were prepared using a Leica VT1200S vibratome as described previously (14). Slices were maintained before experimentation at room temperature for at least 2 hours in ACSF containing the following: 118 mM NaCl, 3.5 mM KCl, 2.5 mM $CaCl_2$, 1.3 mM $MgSO_4$, 1.25 mM NaH_2PO_4, and 15 mM glucose, bubbled with 95% O_2/5% CO_2. WT, Tg19959, $eEF2K^{+/-}$, and Tg19959/$eEF2K^{+/-}$ slices were incubated in puromycin (1 μg/ml) for 1 hour at 32°C in bubbling ACSF. Slices were then flash-frozen on dry ice, and area CA1 was microdissected for Western blot analysis. Puromycin-labeled proteins were identified using the mouse monoclonal antibody 12D10 (1:5000; EMD Millipore, catalog MABE343). Protein synthesis levels were determined by analyzing total lane density from 10 kDa to 250 kDa. Densitometric analysis was performed using Bio-Rad ImageLab software.

Nissl stain. Brains were embedded in paraffin, sectioned at 5 μm thickness, and mounted on charged slides. Sections were cleared in xylene and rehydrated in a graded ethanol series. Slides were stained in 0.1% cresyl violet for 10 minutes and differentiated for 12 minutes in 95% ethanol. Sections were dehydrated through an ethanol series and cleared in xylene before being coverslipped with Vectamount Permanent Mounting Medium. Slides were imaged at ×2 and ×20 on a Keyence BZ-X710 microscope. Hippocampal area was measured and quantified using ImageJ.

Mouse tissue immunohistochemistry. Paraffin-embedded sections (5 μm) mounted on charged slides were cleared in xylene and rehydrated through a graded ethanol series. Sections were pretreated in boiling citrate buffer for 10 minutes and blocked in 3% H_2O_2 for 25 minutes. To reduce nonspecific signals, sections were blocked using the Vector M.O.M. Kit according to the manufacturer's specifications (Vector Labs, catalog BMK-2202). Primary antibody 6E10 (mouse monoclonal; 1:200; BioLegend, catalog SIG-39320) was incubated overnight at 4°C in a humid chamber. A mouse monoclonal IgG isotope antibody (Cell Signaling Technology, catalog 5415) was used for negative control staining in Tg19959 sections to evaluate nonspecific binding of the primary antibody (Supplemental Figure 3A). Following secondary antibody, sections were incubated in ABC reagent (Vectastain ABC Kit; Vector Labs, catalog PK-4000) followed by DAB solution (ImmPACT DAB; Vector Labs, catalog SK-4105) according to the manufacturer's instructions. Sections were dehydrated through a graded ethanol series, cleared in xylene, and coverslipped with Vecta-Mount Permanent Mounting Medium. Slides were imaged at ×2, ×20, and ×60 on a Keyence BZ-X710 microscope. Hippocampal and somatosensory cortical regions were blinded and quantified. Densitometric analysis was performed using ×2 images and ImageJ software.

Postmortem human tissue immunohistochemistry. Postmortem tissue sections from patients were prepared at the University of Washington. Brains were fixed in 10% neutral buffered formalin. Hippocampal samples were embedded in paraffin and sectioned at 5 μm thickness. Sections were mounted on positively charged slides and baked for 30 minutes at 60°C. For staining, sections were deparaffinized in xylene and rehydrated through a graded alcohol series. Slides were boiled in citrate buffer (pH 6.0) for antigen retrieval. Endogenous peroxidase activity was blocked using 3% hydrogen peroxide for 25 minutes. Slides were incubated in a humid chamber in primary antibody for phospho-eEF2 (1:100, Cell Signaling Technology, catalog 2331) overnight at 4°C. Sections were then incubated in biotinylated α-rabbit secondary antibody (1: 200; Vector Labs, catalog PI-1000) for 30 minutes at room temperature followed by Vectastain Elite ABC Reagent (Vector Labs, PK-4000) for another 30 minutes. Primary and secondary antibodies and ABC reagent were diluted in 1% BSA/PBS. Diaminobenzidine (DAB) was diluted in Tris buffer (pH 7.7) and 3% hydrogen peroxidase in a working DAB solution. Sections were developed in DAB for 10 minutes in a 42°C water bath. Slides were counterstained using Mayer's hematoxylin and blued with 0.2% lithium carbonate. Negative controls were incubated in 1% BSA with rabbit IgG as the primary antibody. Sections were dehydrated in an alcohol series and

cleared with xylene, coverslipped, and dried overnight. Slides were imaged at ×20 and ×60 on a Keyence BZ-X710 microscope.

Aβ ELISA. Frozen mouse forebrain samples were sonicated as previously described (14). Samples were centrifuged at 16,000 *g* for 20 minutes at 4°C, and supernatant was collected for ELISA. Aβ 1–42 (Thermo Fisher Scientific, catalog KMB3441) and Aβ 1–40 (Thermo Fisher Scientific, catalog KMB3481) sandwich ELISAs were performed according to the manufacturer's instructions. Anti-rabbit HRP-conjugated secondary antibodies and chromogen dye were used to visualize amyloid peptide levels. 96-Well plates were read at 450 nm using an iMark microplate reader (Bio-Rad).

Drug treatments. Drugs were prepared as stock solutions in either DMSO or dH_2O and diluted into ACSF to a final concentration before experiments. For hippocampal slices, drug incubation was performed at 30–32°C in either a recording chamber or a submersion maintenance chamber containing ACSF saturated with bubbling 95% O_2 and 5% CO_2. The final concentration and sources were as follows: anisomycin (40 μM; Tocris Bioscience, catalog 1290) and puromycin (1 μg/ml; Thermo Fisher Scientific, catalog A1113803).

MS. Hippocampi were dissected and flash-frozen on dry ice. Tissue was lysed in PBS with protease/phosphatase inhibitors using a Bead Mill Homogenizer (Bead Ruptor, Omni International), 500 μl of ×2 RIPA buffer was added, and the mixture was incubated on ice for 30 minutes. Tubes were centrifuged at 18,000 *g* for 10 minutes, and the supernatant was used for analysis. Protein concentration was measured by BCA analysis, and 100 μg of protein was subjected to tryptic digestion.

Reducing alkylation was performed in the presence of 10 mM dithiothreitol and 30 mM iodoacetamide. Samples were incubated overnight at –20°C with cold acetone (4 times the volume of the sample). Protein was pelleted by centrifugation at 14,000 *g* for 10 minutes. After removal of supernatant, the pellet was dried by evaporation of residual acetone for 10 minutes at room temperature and suspended in 50 mM ammonium bicarbonate. The protein suspension was incubated with trypsin at a 1:50 enzyme-to-substrate ratio at 37 °C overnight. The resulting peptides were desalted using a C18 spin column. Purified peptide mixture was prepared in 5% (v/v) ACN containing 1% (v/v) formic acid for liquid chromatography–tandem MS (LC-MS/MS) analysis.

The LC-MS/MS system consisted of a Q Exactive HF Hybrid Quadrupole-Orbitrap Mass Spectrometer (Thermo Fisher Scientific) and a Dionex UltiMate 3000 nano-UPLC system (Thermo Fisher Scientific) employing a Nanospray Flex Ion Source (Thermo Fisher Scientific). An Acclaim PepMap 100 (C18, 5 μm, 100 Å, 100 μm × 2 cm) trap column and an Acclaim PepMap RSLC (C18, 2 μm, 100 Å, 75 μm × 50 cm) analytical column were used for the stationary phase. Good chromatographic separation was observed with a linear gradient consisting of mobile phases A (water with 0.1% formic acid) and B (acetonitrile with 0.1% formic acid), with the gradient ranging from 5% B at 0 minutes to 40% B at 170 minutes. MS spectra were acquired by data-dependent scans consisting of MS/MS scans of the 20 most intense ions from the full MS scan, with a dynamic exclusion option of 10 seconds.

Spectra were searched using the Sequest HT algorithm within the Proteome Discoverer v2.1 (Thermo Fisher Scientific) in combination with the mouse UniProt protein FASTA database (annotated 16,747 entries, December 2015). Search parameters were as follows: FT-trap instrument, parent mass error tolerance of 10 ppm, fragment mass error tolerance of 0.02 Da (monoisotopic), variable modifications of 16 Da (oxidation) on methionine, and fixed modification of 57 Da (carbamidomethylation) on cysteine.

Statistics. Data are presented as mean ± SEM. Summary data are presented as group means with SE bars. For comparisons between 2 groups, a 2-tailed independent Student's *t* test was performed using Prism 6 statistics software (GraphPad Software). Two-tailed paired *t* tests were performed for within-group analyses. For comparisons among more than 2 groups, 1-way ANOVA was used with Tukey's post hoc tests for multiple comparisons. One-way repeated measures ANOVA was used where appropriate, with Tukey's post hoc tests for multiple comparisons. Error probabilities of $P < 0.05$ were considered statistically significant. For MS, error probabilities of $P < 0.08$ were considered statistically significant.

Study approval. All protocols involving animals were approved by the Institutional Animal Care and Use Committee of Wake Forest University School of Medicine. Mice were kept in compliance with the NIH *Guide for the Care and Use of Laboratory Animals* (National Academies Press, 2011). Samples of human tissue were collected in accordance with approved Institutional Review Board protocols. All patients gave informed consent.

Author contributions

BCB conceptualized experiments, collected and analyzed data, and wrote the manuscript. WY, NPK, HRZ, and XZ collected and analyzed data. CDK advised on pathology and provided human tissue samples. AGR provided *eEF2K*$^{-/-}$ mice. TM conceptualized experiments and wrote the manuscript.

Acknowledgments

We thank George Carlson of McLaughlin Research Institute for providing breeders for Tg19959 AD model mice. We thank Cristina M. Furdui and Jingyun Lee (Wake Forest School of Medicine) for technical help on MS analysis. We thank Allison Beller of the University of Washington School of Medicine for administrative support and Kim Howard for technical support with human tissue samples. We thank Kenneth Grant (Wake Forest School of Medicine) for technical help on TEM imaging. We thank staff of the Wake Forest School of Medicine Pathology Core for their help with tissue processing for immunohistochemistry. We also acknowledge the editorial assistance of Karen Klein in the Wake Forest Clinical and Translational Science Institute (UL1 TR001420; principal investigator, McClain). This work was supported by NIH grants K99/R00 AG044469, R01 AG055581, R01 AG056622 (to TM), F31AG055264 (to HRZ), F31AG054113 (to BCB), P50AG005136 (University of Washington Alzheimer's Disease Research Center), U01AG006781 (University of Washington Adult Changes in Thought study), Alzheimer's Association grant NIRG-15-362799 (to TM), BrightFocus Foundation grant A2017457S, Wake Forest Alzheimer's Disease Core Center (ADCC) pilot grant P30AG049638 (to TM), Wake Forest Clinical and Translational Science Institute (CTSI) pilot grant (to TM), and the Nancy and Buster Alvord Endowment (to CDK).

Address correspondence to: Tao Ma, Department of Internal Medicine-Gerontology and Geriatric Medicine, Wake Forest School of Medicine, Medical Center Boulevard, Winston-Salem, North Carolina 27157, USA. Phone: 336.716.4981; Email: tma@wakehealth.edu.

1. Selkoe DJ. Alzheimer's disease is a synaptic failure. *Science*. 2002;298(5594):789–791.
2. Mochida H, Sato K, Sasaki S, Yazawa I, Kamino K, Momose-Sato Y. Effects of anisomycin on LTP in the hippocampal CA1: long-term analysis using optical recording. *Neuroreport*. 2001;12(5):987–991.
3. Remaud J, et al. Anisomycin injection in area CA3 of the hippocampus impairs both short-term and long-term memories of contextual fear. *Learn Mem*. 2014;21(6):311–315.
4. Rossato JI, Bevilaqua LR, Myskiw JC, Medina JH, Izquierdo I, Cammarota M. On the role of hippocampal protein synthesis in the consolidation and reconsolidation of object recognition memory. *Learn Mem*. 2007;14(1):36–46.
5. Costa-Mattioli M, Sossin WS, Klann E, Sonenberg N. Translational control of long-lasting synaptic plasticity and memory. *Neuron*. 2009;61(1):10–26.
6. Buffington SA, Huang W, Costa-Mattioli M. Translational control in synaptic plasticity and cognitive dysfunction. *Annu Rev Neurosci*. 2014;37:17–38.
7. Langstrom NS, Anderson JP, Lindroos HG, Winblad B, Wallace WC. Alzheimer's disease-associated reduction of polysomal mRNA translation. *Brain Res Mol Brain Res*. 1989;5(4):259–269.
8. Ding Q, Markesbery WR, Chen Q, Li F, Keller JN. Ribosome dysfunction is an early event in Alzheimer's disease. *J Neurosci*. 2005;25(40):9171–9175.
9. Hernández-Ortega K, Garcia-Esparcia P, Gil L, Lucas JJ, Ferrer I. Altered machinery of protein synthesis in Alzheimer's: from the nucleolus to the ribosome. *Brain Pathol*. 2016;26(5):593–605.
10. Moreno JA, et al. Oral treatment targeting the unfolded protein response prevents neurodegeneration and clinical disease in prion-infected mice. *Sci Transl Med*. 2013;5(206):206ra138.
11. Radford H, Moreno JA, Verity N, Halliday M, Mallucci GR. PERK inhibition prevents tau-mediated neurodegeneration in a mouse model of frontotemporal dementia. *Acta Neuropathol*. 2015;130(5):633–642.
12. Proud CG. Regulation and roles of elongation factor 2 kinase. *Biochem Soc Trans*. 2015;43(3):328–332.
13. Ryazanov AG, Davydova EK. Mechanism of elongation factor 2 (EF-2) inactivation upon phosphorylation. Phosphorylated EF-2 is unable to catalyze translocation. *FEBS Lett*. 1989;251(1–2):187–190.
14. Ma T, et al. Inhibition of AMP-activated protein kinase signaling alleviates impairments in hippocampal synaptic plasticity induced by amyloid β. *J Neurosci*. 2014;34(36):12230–12238.
15. Jan A, et al. eEF2K inhibition blocks Aβ42 neurotoxicity by promoting an NRF2 antioxidant response. *Acta Neuropathol*. 2017;133(1):101–119.
16. Schmidt EK, Clavarino G, Ceppi M, Pierre P. SUnSET, a nonradioactive method to monitor protein synthesis. *Nat Methods*. 2009;6(4):275–277.
17. Ma T, et al. Suppression of eIF2α kinases alleviates Alzheimer's disease-related plasticity and memory deficits. *Nat Neurosci*. 2013;16(9):1299–1305.
18. Antunes M, Biala G. The novel object recognition memory: neurobiology, test procedure, and its modifications. *Cogn Process*. 2012;13(2):93–110.
19. Leger M, et al. Object recognition test in mice. *Nat Protoc*. 2013;8(12):2531–2537.
20. Vogel-Ciernia A, Wood MA. Examining object location and object recognition memory in mice. *Curr Protoc Neurosci*. 2014;69:8.31.1–8.3117.
21. Ma T, Klann E. Amyloid β: linking synaptic plasticity failure to memory disruption in Alzheimer's disease. *J Neurochem*. 2012;120 Suppl 1:140–148.
22. Shankar GM, et al. Amyloid-beta protein dimers isolated directly from Alzheimer's brains impair synaptic plasticity and memory. *Nat Med*. 2008;14(8):837–842.
23. Koffie RM, Hyman BT, Spires-Jones TL. Alzheimer's disease: synapses gone cold. *Mol Neurodegener*. 2011;6(1):63.
24. Hering H, Sheng M. Dendritic spines: structure, dynamics and regulation. *Nat Rev Neurosci*. 2001;2(12):880–888.
25. Sala C, Segal M. Dendritic spines: the locus of structural and functional plasticity. *Physiol Rev*. 2014;94(1):141–188.
26. Scheff SW, Price DA, Schmitt FA, Mufson EJ. Hippocampal synaptic loss in early Alzheimer's disease and mild cognitive impairment. *Neurobiol Aging*. 2006;27(10):1372–1384.
27. Sutton MA, Schuman EM. Dendritic protein synthesis, synaptic plasticity, and memory. *Cell*. 2006;127(1):49–58.
28. Risher WC, Ustunkaya T, Singh Alvarado J, Eroglu C. Rapid Golgi analysis method for efficient and unbiased classification of dendritic spines. *PLoS One*. 2014;9(9):e107591.
29. Okabe S. Molecular anatomy of the postsynaptic density. *Mol Cell Neurosci*. 2007;34(4):503–518.
30. Ostroff LE, Watson DJ, Cao G, Parker PH, Smith H, Harris KM. Shifting patterns of polyribosome accumulation at synapses over the course of hippocampal long-term potentiation. *Hippocampus*. 2018;28(6):416–430.
31. Ostroff LE, Fiala JC, Allwardt B, Harris KM. Polyribosomes redistribute from dendritic shafts into spines with enlarged synapses during LTP in developing rat hippocampal slices. *Neuron*. 2002;35(3):535–545.
32. Radde R, et al. Abeta42-driven cerebral amyloidosis in transgenic mice reveals early and robust pathology. *EMBO Rep*. 2006;7(9):940–946.
33. Hardie DG. AMPK--sensing energy while talking to other signaling pathways. *Cell Metab*. 2014;20(6):939–952.
34. Vingtdeux V, Chandakkar P, Zhao H, d'Abramo C, Davies P, Marambaud P. Novel synthetic small-molecule activators of AMPK as enhancers of autophagy and amyloid-β peptide degradation. *FASEB J*. 2011;25(1):219–231.
35. Lin MT, Beal MF. Mitochondrial dysfunction and oxidative stress in neurodegenerative diseases. *Nature*. 2006;443(7113):787–795.
36. Massaad CA, Washington TM, Pautler RG, Klann E. Overexpression of SOD-2 reduces hippocampal superoxide and prevents memory deficits in a mouse model of Alzheimer's disease. *Proc Natl Acad Sci U S A*. 2009;106(32):13576–13581.
37. Paschen W, Proud CG, Mies G. Shut-down of translation, a global neuronal stress response: mechanisms and pathological relevance. *Curr Pharm Des*. 2007;13(18):1887–1902.
38. Wek RC, Cavener DR. Translational control and the unfolded protein response. *Antioxid Redox Signal*. 2007;9(12):2357–2371.
39. Leprivier G, et al. The eEF2 kinase confers resistance to nutrient deprivation by blocking translation elongation. *Cell*. 2013;153(5):1064–1079.
40. Klann E, Sweatt JD. Altered protein synthesis is a trigger for long-term memory formation. *Neurobiol Learn Mem*. 2008;89(3):247–259.
41. Browne GJ, Proud CG. Regulation of peptide-chain elongation in mammalian cells. *Eur J Biochem*. 2002;269(22):5360–5368.
42. Graber TE, McCamphill PK, Sossin WS. A recollection of mTOR signaling in learning and memory. *Learn Mem*. 2013;20(10):518–530.
43. Trinh MA, Klann E. Translational control by eIF2α kinases in long-lasting synaptic plasticity and long-term memory. *Neurobiol Learn Mem*. 2013;105:93–99.
44. Beckelman BC, Zhou X, Keene CD, Ma T. Impaired eukaryotic elongation factor 1A expression in Alzheimer's disease. *Neurodegener Dis*. 2016;16(1–2):39–43.
45. Beckelman BC, et al. Dysregulation of elongation factor 1A expression is correlated with synaptic plasticity impairments in Alzheimer's disease. *J Alzheimers Dis*. 2016;54(2):669–678.
46. Heise C, et al. eEF2K/eEF2 pathway controls the excitation/inhibition balance and susceptibility to epileptic seizures. *Cereb Cortex*. 2017;27(3):2226–2248.
47. Taha E, Gildish I, Gal-Ben-Ari S, Rosenblum K. The role of eEF2 pathway in learning and synaptic plasticity. *Neurobiol Learn Mem*. 2013;105:100–106.
48. Zimmermann HR, et al. Genetic removal of eIF2α kinase PERK in mice enables hippocampal L-LTP independent of mTORC1 activity. *J Neurochem*. 2018;146(2):133–144.
49. Liu R, Proud CG. Eukaryotic elongation factor 2 kinase as a drug target in cancer, and in cardiovascular and neurodegenerative diseases. *Acta Pharmacol Sin*. 2016;37(3):285–294.
50. Verpelli C, et al. Synaptic activity controls dendritic spine morphology by modulating eEF2-dependent BDNF synthesis. *J Neurosci*. 2010;30(17):5830–5842.
51. Sutton MA, Taylor AM, Ito HT, Pham A, Schuman EM. Postsynaptic decoding of neural activity: eEF2 as a biochemical sensor coupling miniature synaptic transmission to local protein synthesis. *Neuron*. 2007;55(4):648–661.
52. Heise C, Gardoni F, Culotta L, di Luca M, Verpelli C, Sala C. Elongation factor-2 phosphorylation in dendrites and the regulation of dendritic mRNA translation in neurons. *Front Cell Neurosci*. 2014;8:35.
53. Korol' TY, Korol' SV, Kostyuk EP, Kostyuk PG. Disruption of calcium homeostasis in Alzheimer's disease. *Neurophysiology*. 2008;40(5–6):385–392.
54. Popugaeva E, Pchitskaya E, Bezprozvanny I. Dysregulation of neuronal calcium homeostasis in Alzheimer's disease - A therapeutic opportunity? *Biochem Biophys Res Commun*. 2017;483(4):998–1004.
55. Riascos D, et al. Age-related loss of calcium buffering and selective neuronal vulnerability in Alzheimer's disease. *Acta Neuropathol*. 2011;122(5):565–576.
56. Brittain JM, Wang Y, Wilson SM, Khanna R. Regulation of CREB signaling through L-type

Ca2+ channels by Nipsnap-2. *Channels (Austin)*. 2012;6(2):94–102.
57. Mackenzie IR, Neumann M. Molecular neuropathology of frontotemporal dementia: insights into disease mechanisms from postmortem studies. *J Neurochem*. 2016;138(Suppl 1):54–70.
58. Garcia-Esparcia P, et al. Dementia with Lewy bodies: molecular pathology in the frontal cortex in typical and rapidly progressive forms. *Front Neurol*. 2017;8:89.
59. Braak H, Braak E. Neuropathological stageing of Alzheimer-related changes. *Acta Neuropathol*. 1991;82(4):239–259.
60. Mirra SS, et al. The Consortium to Establish a Registry for Alzheimer's Disease (CERAD). Part II. Standardization of the neuropathologic assessment of Alzheimer's disease. *Neurology*. 1991;41(4):479–486.
61. Chu HP, et al. Germline quality control: eEF2K stands guard to eliminate defective oocytes. *Dev Cell*. 2014;28(5):561–572.
62. Chishti MA, et al. Early-onset amyloid deposition and cognitive deficits in transgenic mice expressing a double mutant form of amyloid precursor protein 695. *J Biol Chem*. 2001;276(24):21562–21570.
63. Park S, et al. Elongation factor 2 and fragile X mental retardation protein control the dynamic translation of Arc/Arg3.1 essential for mGluR-LTD. *Neuron*. 2008;59(1):70–83.